JACS
JOURNAL OF THE AMERICAN CHEMICAL SOCIETY
pubs.acs.org/JACS
Article

Superconductivity of 30.4 K and Its Reemergence under Pressure in $Fe_{1.11}Se$ Synthesized via Ion-Exchange and Deintercalation Reaction

Mingzhang Yang,[▽] Yuxin Ma,[▽] Qi Li, Ke Ma, Jiali Lu, Zhaolong Liu, Ruijin Sun, Tianping Ying, Mengdi Wang, Xin Chen, Changchun Zhao, Jian-gang Guo,* Shifeng Jin,* and Xiaolong Chen*

Cite This: J. Am. Chem. Soc. 2026, 148, 6695−6703

Read Online

ACCESS | Metrics & More | Article Recommendations | Supporting Information

ABSTRACT: Binary stoichiometry FeSe (*s*-FeSe) is a well-known parent of high-temperature unconventional superconductors owing to its charge-neutral layer, highly tunable structure and electronic properties, and rich interplay among multiple electronic phases. Yet, the *s*-FeSe synthesized via high-temperature equilibrium reactions bears the notorious interstitial Fe, where merely 3% of them is sufficient to kill the superconductivity. Here, we successfully synthesized a new nonstoichiometric $Fe_{1.11}Se$ single crystal with a superconducting onset temperature (T_c^{onset}) of 30.4 K through a hydrothermal ion-exchange and deintercalation route. 11% interstitial Fe ions exceed the equilibrium phase diagram limit. Intriguingly, under physical pressure, the T_c^{onset} of $Fe_{1+\delta}Se_{1-x}S_x$ exhibits a "V"-shaped evolution with a minimum at 2−2.6 GPa and then upturning into a second superconducting region, reminiscent of the behaviors in FeSe-intercalates. Furthermore, a pressure-induced possible magnetic order, previously observed only in pressurized *s*-FeSe, shows up. These results offer fresh insights into the role of interstitial Fe in governing superconducting and transport properties under nonequilibrium synthesis and tuning strategies.

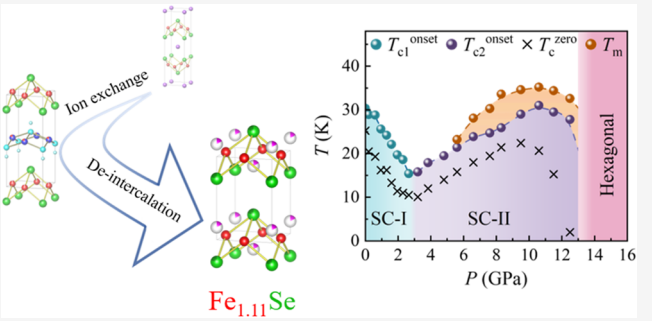

INTRODUCTION

FeSe-based superconductors have become an exceptional member in the iron-based superconducting family on account of highly tunable layered structures,[1−3] the highest critical temperature (T_c),[4] and topological surface state for potential applications in quantum computing,[5−7] etc. Stoichiometric FeSe (*s*-FeSe) synthesized by high-temperature sintering of 1000−1200 K, i.e., equilibrium-state synthesis method, exhibits a modest T_c of 8.5 K.[8] Its superconductivity (SC) is extremely sensitive to Fe content, which is fully suppressed by mere 3% interstitial Fe.[8] Partial substitution of Se by S/Te in *s*-FeSe slightly enhances T_c to 12−15 K,[9−12] simultaneously bringing out competing or intertwining phenomena including magnetic fluctuations, quantum critical point, and rich electronic phases.[13−15]

In the past few years, to enhance T_c and explore the superconducting mechanism of FeSe, researchers have dedicated major efforts to three categories of nonequilibrium approaches. The first involves chemical or electrochemical intercalation of structural units, by which alkali-metal ions (K^+, Rb^+, Cs^+),[16−20] inorganic−organic molecule groups $[Li_x(NH_3)_y$, $K_x(NH_3)_y$, $Na_x(NH_3)_y$, $Na_x(C_2H_8N_2)_y]$,[21−25] and inorganic hydroxide $(Li_yFe_{1-y}OH)^{\delta+}$ are inserted between FeSe layers.[26,27] These FeSe-intercalates exhibit the highest T_c of 46 K, exceeding the McMillan limited temperature of the BCS theory framework. The second strategy is directly depositing one-unit-cell FeSe on the $SrTiO_3$ substrate, in which much higher T_c values of 65−100 K are achieved.[4,28,29] The synergistic effect of interface charge transfer and the phonon vibration of oxygen is responsible for the remarkable enhancement of T_c. The third method is employing physical pressure to tune the atomic arrangements and configurations in favor of enhancing SC in a relatively simple way. The T_c of *s*-FeSe increases monotonically to 37 K at 6−8 GPa and then decreases, forming a dome-shaped superconducting zone.[30−33] Above 10 GPa, the superconducting anti-PbO FeSe changes into the nonsuperconducting NiAs phase. Notably, at 2−6 GPa, a new stripe-type antiferromagnetic (S-AFM) transition emerges, likely competing with the SC.[34,35] Besides, the FeSe-intercalates are also pressurized, and their T_cs can be enhanced above 50 K in re-entrant superconducting phases.[36−39] These studies indicate that effective electron doping and modifications to the $FeSe_4$ tetrahedral environment, either individually or jointly, play essential roles in enhancing SC and producing emergent electronic states.

Received: December 18, 2025
Revised: January 23, 2026
Accepted: January 29, 2026
Published: February 4, 2026

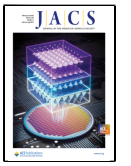

https://doi.org/10.1021/jacs.5c22761
J. Am. Chem. Soc. 2026, 148, 6695−6703

Here, we develop a two-step hydrothermal ion-exchange and deintercalation route to synthesize new $Fe_{1.11}Se$ bulk single crystals having 11% interstitial Fe2 ions, which is much higher than its solubility in the Fe−Se binary phase diagram. Remarkably, this new nonstoichiometric $Fe_{1.11}Se$ exhibits a T_c^{onset} of 30.4 K, identical to that in $K_xFe_2Se_2$. The Fe2 thus acts as a benign dopant, which suppresses nematicity, injects electrons, and enhances SC. More interestingly, T_c is suppressed to a minimal value near 2.5 GPa in the SC-I zone and then enhanced to a maximal value under pressure, forming a SC-II zone. In terms of superconducting evolution, such a V-shaped T_c is totally different from single-dome SC in *s*-FeSe, while it resembles those of FeSe-intercalates. In the SC-II zone, an emergent possible magnetic phase coexists with an SC above 5.6 GPa. The new pressure-dependent electronic property seems bridge the gap between *s*-FeSe and FeSe-intercalates.

RESULTS AND DISCUSSION

Single crystals of $Fe_{1+\delta}Se_{1-x}S_x$ (x = 0, 0.3, 0.6) were successfully synthesized by the hydrothermal intercalation and selective deintercalation procedure, see Figure 1a. Single-crystal X-ray diffraction (SCXRD) on a 152 × 66 × 11 μm^3 specimen at 299 K shows that $Fe_{1.11}Se$ crystallizes in the LiFeAs-type structure with a space group of $P4/nmm$.[40] Fe1 and Se fully occupy the 2b [1/4, 3/4, 1/2] and 2c [1/4, 1/4, 0.266(1)] Wyckoff sites. Differential Fourier maps reveal residual electron density between layers, attributed to interstitial Fe2 ions with an occupancy of 11%, which randomly occupy the 2c site [1/4, 1/4, 0.866(1)]. More details are shown in Table S1 and Figure S1.

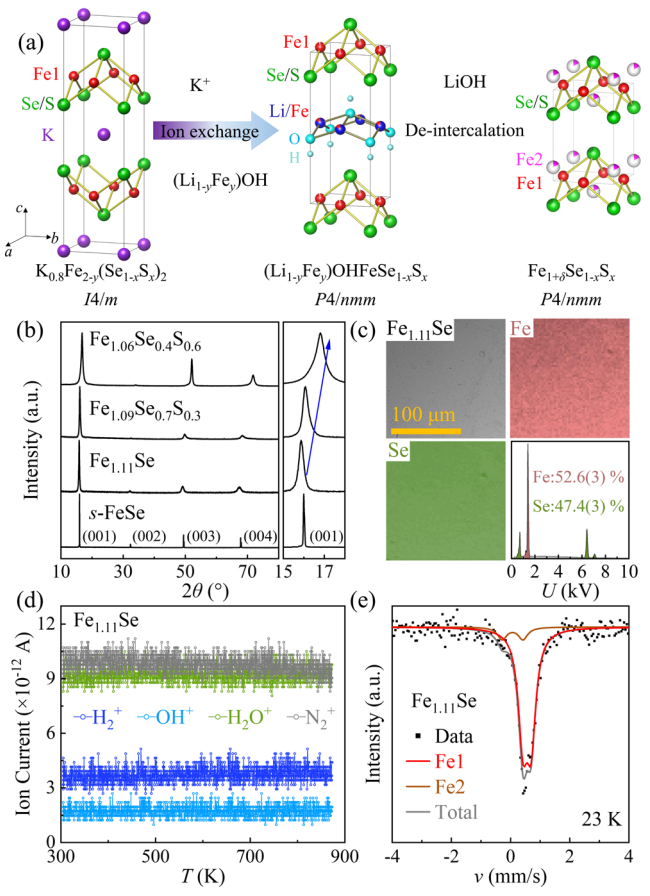

Figure 1. (a) Schematic synthesis route and crystal structure of $Fe_{1+\delta}Se_{1-x}S_x$. (b) Powder X-ray diffraction patterns of *s*-FeSe and $Fe_{1+\delta}Se_{1-x}S_x$ single crystals. (c) SEM image and EDX mapping of $Fe_{1.11}Se$. (d) Dynamic gas composition analysis of $Fe_{1.11}Se$. (e) ^{57}Fe Mössbauer spectrum of $Fe_{1.11}Se$ at 23 K.

The purity of the single-crystal form is also examined by powder X-ray diffraction (PXRD) on a 0.5 × 0.3 cm^2 specimen, showing only sharp (00l) reflections and no detectable peaks of precursors $K_{0.8}Fe_{2-y}(Se_{1-x}S_x)_2$ and $(Li_{1-y}Fe_y)OHFeSe_{1-x}S_x$. Notably, the lowest-angle Bragg reflection corresponds to a d-spacing of 5.588(6) Å, 1.2% larger than that of *s*-FeSe. It implies the incorporation of additional species between adjacent FeSe layers. Upon sulfur doping, all (00l) peaks shift to a higher angle. More details from the refinement are given in Table S2.

The elemental compositions of $Fe_{1.11}Se$ crystals were determined by using several characterization techniques. The complete deintercalation of K^+ or Li^+ can be confirmed by inductively coupled plasma-atomic emission spectroscopy (ICP-AES) and energy-dispersive X-ray spectroscopy (EDX) (see Figure 1c). The Fe/Se ratio measured by ICP-AES is 1.18(1):1. The EDX elemental mapping on freshly cleaved crystal surfaces (Figure 1c), which shows a homogeneous distribution of Fe and Se with the Fe/Se ratio of 1.11(1):1, is in good agreement with the analysis of SCXRD measurements. The ratio of Fe/Se is determined as 1.09(1):1 and 1.06(1):1 for x = 0.3 and 0.6, respectively. We further performed *in situ* dynamic gas composition analysis using a quadrupole mass spectrometer (QMS). As shown in Figure 1d, the H_2^+ signal is 3.5 × 10^{-12} A up to 870 K, which is smaller than the background N_2 signal. There are also negligible water-derived signals, i.e., OH^+ and H_2O^+, below 5 × 10^{-12} A.

To further confirm the presence and local environment of Fe2 in $Fe_{1.11}Se$, we conducted a ^{57}Fe Mössbauer spectrum at 23 K. The primary doublet (Fe1) exhibits an isomer shift (IS) of 0.56(1) mm·s^{-1} and a quadrupole splitting of 0.28(1) mm·s^{-1}, which are nearly equal to that of *s*-FeSe (IS = 0.57(1) mm·s^{-1}, QS = 0.30(1) mm·s^{-1} at 5 K).[8] The isomer shift of Fe2 ion in $Fe_{1.11}Se$ is 0.07 mm·s^{-1}, which is lightly lower than the 0.14−0.2 mm·s^{-1} of Fe2 ions in $Fe_{1.125}Te$. However, no additional doublets or magnetic splitting is observed in the spectrum, contrasting with the magnetic ordering of $Fe_{1+x}Te$ ($x \geq 0.14$).[41,42] The interstitial Fe2 in $Fe_{1.11}Se$ should be nonmagnetic and may locate at a less symmetric surrounding. Besides, the relative ratio of spectral areas for Fe1/Fe2 is 1:0.12(2), which quantitatively matches the 11% interstitial Fe2. Based on these observations, we can thus conclude that the existence of 11% Fe2 is reasonable. In addition, the effective moment of Fe2 is 4.9(1) μ_B (S = 2, tetrahedral d^6) derived from temperature-dependent magnetic susceptibility as shown in Figure S2.

The electrical transport properties of $Fe_{1+\delta}Se_{1-x}S_x$ (x = 0, 0.3, 0.6) were measured at ambient pressure as shown in Figure 2a. The $\rho-T$ curves of three samples do not have any kinks, suggesting the absence of the nematic phase of *s*-FeSe. At lower temperatures, the sharp drop of ρ due to the superconducting transition emerges. We plot them in Figure 2b, where the T_c^{onset} of $Fe_{1.11}Se$ is 30.4 K, which is nearly four times higher than that of *s*-FeSe. The T_c^{onset} decreases to 17.4 and 12.2 K in $Fe_{1.09}Se_{0.7}S_{0.3}$ and $Fe_{1.06}Se_{0.4}S_{0.6}$, respectively. We fitted the normal-state $\rho-T$ curves from T_c^{onset} to 80 K by $\rho(T) = \rho_0 + AT^{\alpha}$, as shown in Figure 1a. All α values are close

https://doi.org/10.1021/jacs.5c22761
J. Am. Chem. Soc. 2026, 148, 6695−6703

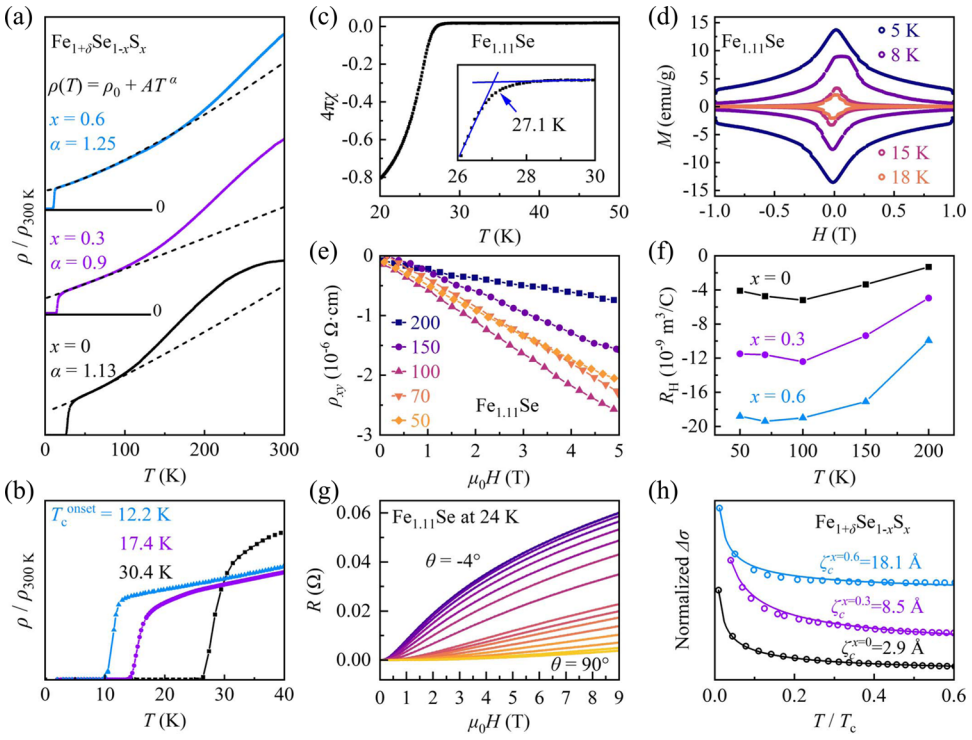

Figure 2. (a) Temperature dependence of normalized electrical resistivity (ρ/ρ_{300K}) of $Fe_{1+\delta}Se_{1-x}S_x$. Black, violet, and blue curves are x = 0, 0.3, and 0.6, respectively. Black dashed lines are the fitting curves. (b) Superconducting transition of $Fe_{1+\delta}Se_{1-x}S_x$. (c) Zero-field-cooled magnetization (ZFC) of $Fe_{1.11}Se$ at 10 Oe, and the inset is a zoom-in transition. (d) $M-H$ curves of $Fe_{1.11}Se$. (e) Hall resistivity of $Fe_{1.11}Se$ as a function of magnetic fields. (f) Temperature-dependent Hall coefficient R_H of $Fe_{1+\delta}Se_{1-x}S_x$. (g) Magnetic field dependence of the resistance for $Fe_{1.11}Se$ at 24 K under varying angles. (h) Normalized $\Delta\sigma_{0T}$ derived from the Lawrence−Doniach (LD) model of three samples.

to 1, indicating the non-Fermi-liquid behaviors. Magnetic measurements under ZFC conditions demonstrated the bulk SC in $Fe_{1.11}Se$. In Figure 2c, a sharp diamagnetic transition shows a T_c^{zero} of 27.1 K at 10 Oe. The magnetization versus magnetic field ($M-H$) curves in Figure 2d exhibit a pronounced hysteresis loop at 5 K, characteristic of type-II superconductivity and strong flux-pinning. The $\rho-T$ curves below 50 K under different H values are presented in Figure S3. The "tail" of resistivity seems like the behavior in those 2D superconductors.[43,44] Figure 2e displays the linear field-dependent ρ_{xy} up to 5 T at 50−200 K. It shows a single-band model dominated by electrons, which is different from the two-band model in s-FeSe. In all samples, the Hall coefficients R_H are negative, as shown in Figure 2f. The electron concentration $n_e = 1/(R_H \cdot e)$ of $Fe_{1.11}Se$ is $1.28(1) \times 10^{21}$ cm^{-3} at 50 K, which decreases upon doping sulfur. The T_c also decreases as n is lowered.

To probe the interlayer interaction in $Fe_{1.11}Se$, we measured the angular magnetoresistance of $Fe_{1.11}Se$ at 24 K up to 9 T (see Figure 2g). The SC is suppressed as the angle θ between the c-axis and the magnetic field increases from −4° to 90°, indicating anisotropic SC. Further analysis of the fluctuation-induced magnetoconductivity using the 2D Lawrence−Doniach (LD) model reveals that the coherence length (ξ_c) of $Fe_{1.11}Se$ along the c-axis is 2.9 Å, remarkably shorter than ξ_c of 26 Å in s-FeSe.[45,46] Thus, $Fe_{1.11}Se$ is an anisotropic superconductor. Upon sulfur doping, the ξ_c increases to 5.5 and 18.1 Å for x = 0.3 and 0.6, and the anisotropic SC gradually weakens.

We freshly cleaved single crystals for *in situ* electrical transport measurements under pressure. All of the $\rho-T$ curves are shown in Figure 3a,b. The T_c^{onset} of $Fe_{1.11}Se$ initially decreases with applied pressure, reaching a minimum value of 15.4 K at 2.6 GPa in the SC-I zone. Then, it inversely increases to 31.1 K with further compression. As P > 5.5 GPa, a weak kink of the $\rho-T$ curve emerges above T_c^{onset}. It may be a stripe-type antiferromagnetic (S-AFM) transition just observed in pressurized s-FeSe,[32,33,50,51] marked as violet arrow of T_m in Figure 3b. This anomaly can be easily found in the temperature derivative $d\rho/dT$ curves in Figure S4. Interestingly, both T_m and T_c^{onset} increase with increasing P, showing peaks of 35.2 and 31.1 K at 10.6 GPa, respectively. At 12.5 GPa, the resistivity does not reach zero at 1.8 K. As P > 13.6 GPa, neither superconducting nor magnetic transitions are observed. We also measured $\rho-T$ curves of the sulfur-doped samples with x = 0.3 (Figure 3c,d) and 0.6 under pressure (see Figure S4). Their T_c^{onset} shows a similar V-shaped evolution with a minimal T_c^{onset} at ∼2.0 GPa. The T_m transition also emerges as P > 5.5 GPa. For x = 0.3, the highest T_c^{onset} is 25 K at 7.0 GPa. While in x = 0.6, the highest T_c^{onset} of re-entered SC is 8 K at 5.5 GPa. In addition, the tetragonal−hexagonal phase transition in sulfur-doped samples decreases to 12 and 10 GPa, which is reasonably due to the pre-exertion of chemical pressure by doping smaller sulfur ions in $Fe_{1.11}Se$.

To gain more insight into the pressurized SC of $Fe_{1+\delta}Se_{1-x}S_x$, we plot the whole pressure-dependent electronic phase diagram in Figure 4a. In the three diagrams, the T_c^{onset} and T_c^{zero} decrease in the SC-I region and then lower to a minimum at P of 2.0−2.6 GPa, followed by a dome-like T_c in the SC-II. As P > 13.6, 12, and 10 GPa, the SC of the three samples totally disappears, respectively. We first examine whether the structural phase transition exists under pressure. The *in situ* synchrotron diffractions under pressure of x = 0 and x = 0.3 were conducted, and all of the patterns are plotted in

https://doi.org/10.1021/jacs.5c22761
J. Am. Chem. Soc. 2026, 148, 6695−6703

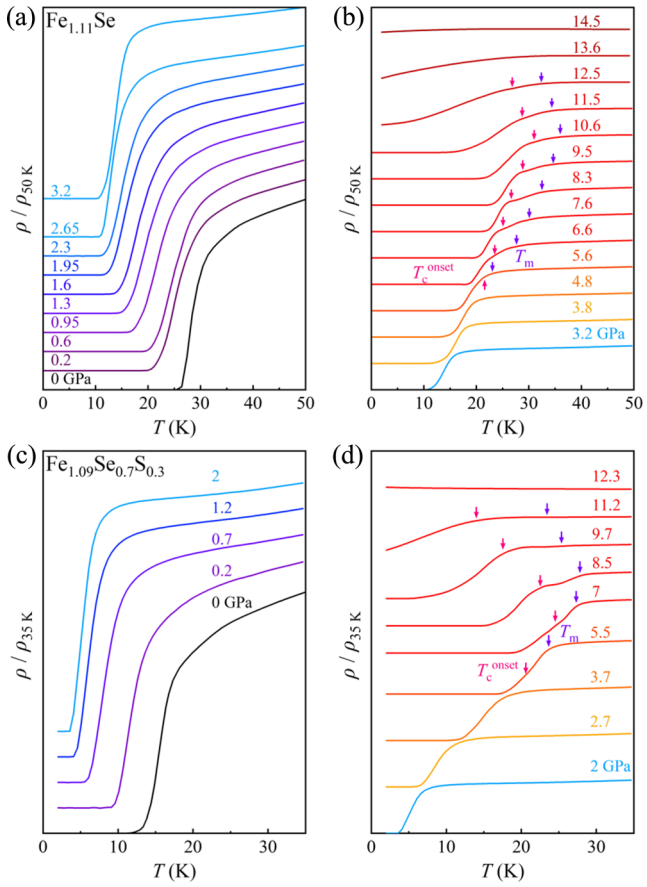

Figure 3. Temperature-dependent ρ/ρ_{50K} and ρ/ρ_{35K} in (a, b) $Fe_{1.11}Se$ and (c, d) $Fe_{1.09}Se_{0.7}S_{0.3}$ single crystals, respectively, under different pressures. The red and violet arrows label the T_c^{onset} and possible magnetic transition T_m, respectively.

Figure S5. The contour plots clearly reveal that no structural transition occurs in the two SC-I and SC-II zones. Further increasing pressure, additional peaks show up, and the phases gradually change into a NiAs-type hexagonal structure. At the same time, the SC and possible magnetic phase transition disappear.

In addition, we plot the pressure-dependent cell volume ratio V/V_{0GPa} and the lattice parameters ratio c/a of $Fe_{1.11}Se$ in Figure 4d,4e, respectively. More details about $Fe_{1.09}Se_{0.7}S_{0.3}$ are plotted in Figure S6. For $Fe_{1.11}Se$, the V/V_{0GPa} and c/a ratio decrease smoothly and rapidly in 0−6 GPa, which are commonly observed in FeSe-intercalates.[38,52] Above 6 GPa, the decrement of V/V_{0GPa} seems to deviate from the standard Birch−Murnaghan (BM) equation of state, and the shrinkage of c/a also slows down. These abnormal behaviors imply the formation of an interlayer bonding state under pressure.

Furthermore, we performed density functional theory (DFT) calculations using the lattice parameters of $Fe_{1.11}Se$ under high pressures. As shown in Figure S7, the Fermi surface (FS) displays a quasi-2D cylindrical shape at 0 GPa. With increasing pressure, the bands along A−M cross the Fermi level, leading to the FS gradually warping toward a spherical form. At 10 GPa, the FS is fully enclosed within the first Brillouin zone, showing 3D character. In Figure S8a, we plotted the change in projected density of states and total density of states under pressure. It can be seen that the contributions of the five orbitals do not change much at E_F. As for the total value, it decreases from 21.42 to 17.54 states/eV as shown in Figure S8b, which does not directly relate to the value of T_c.

We listed the T_c and n_e of $Fe_{1.11}Se$, *s*-FeSe, and three FeSe-intercalates in Table 1. The n_e of $Fe_{1.11}Se$ reached a level comparable to that of FeSe-intercalates with high T_c, indicating the doping effect of interstitial Fe. Furthermore, the $Fe_{1.11}Se$ annealed at 200 °C still keeps the high T_c^{onset} of 28.5 K, slightly lower than pristine $Fe_{1.11}Se$ as plotted in Figure S9. However, the T_c^{onset} of the sample annealed at 400 °C moves down to 9.6 K, identical to that of s-FeSe, indicating that $Fe_{1.11}Se$ is a metastable superconductor sustained at low temperature.

Let us compare our $P-T$ phase diagrams with those in pressurized *s*-FeSe and FeSe-intercalates. In the former case, the nematic transition is suppressed by pressure, and the T_c of 8 K slowly increases to 37 K at ∼6 GPa. Detailed $\rho-T$ measurements confirm that there is a magnetic phase transition between 2−6 GPa. As $P > 6$ GPa, the T_c slowly decreases and vanishes when a NiAs-type nonsuperconducting phase emerges. In $K_xFe_2Se_2$, the T_c of 31 K monotonically decreases to zero near 10 GPa, and then a second superconducting phase re-emerges with T_c of 48 K.[36] This reentrance might be related to a quantum critical point.[37] In $(Li_yFe_{1-y}OH)FeSe$ and $Li_x(NH_3)_yFeSe$, a V-shaped SC is reported, and the minimal T_c occurs at 2−4 GPa.[38,39] However, the magnetic transition is not observed in any of these FeSe-intercalates. As for $Fe_{1.11}Se$, the pressure-dependent V-shaped SC is different from those of *s*-FeSe at lower pressure, while it is similar to the reports in FeSe-intercalates. In addition, at a higher pressure region of 5.6−12.5 GPa, the emergent possible magnetic phase transition is similar to the S-AFM transition in pressurized *s*-FeSe.

As previously reported, this magnetic transition is closely related to a hole pocket located at the center of the Brillouin zone of the reconstructed Fermi surface. However, in $Fe_{1.11}Se$ and FeSe-intercalates, the doped electrons significantly enlarge the electron pockets. This is verified by the Hall measurements in $Fe_{1.11}Se$, where the R_H of -4.86×10^{-9} m^3/C at ambient pressure equals the value of $(Li_yFe_{1-y}OH)FeSe$. Furthermore, all of these values are negative, as shown in Figure 4f, where the data were fitted by the single-band model (see Figure S10). Since the hole pocket in $Fe_{1.11}Se$ should be pretty small, it is unlikely the scenario of hole pocket nesting-induced magnetism in pressurized *s*-FeSe.[33] Alternately, one possible picture is that the interstitial Fe2 ions become magnetically interacting under pressure. Further studies will be of interest to clarify the origin.

In a recent work, the author claimed that the T_c of FeSe-based superconductors is positively correlated with electron concentrations.[47] This statement is supported by the relationship between T_c and carrier concentrations of $Fe_{1+\delta}Se_{1-x}S_x$ at ambient pressure, as shown in Figure 2f and Table 1. Nevertheless, the pressure-induced V-shaped SC is not fully explained by the pressure-dependent carrier concentrations, which monotonically increase with applied pressure. We did not observe critical points at 2−2.6 GPa in Figure 4f. Thus, additional parameters must be taken into consideration.

In addition, double-dome SC was found in many iron-based superconductors like the case of $LaFeAsO_{1-x}H_x$ and pressurized $K_xFe_2Se_2$.[36,37,53,54] In the former, the two-dome structure is closely related to bipartite magnetic parents LaFeAsO and $LaFeAsO_{0.5}H_{0.5}$. Under chemical doping, the two magnetic parents evolve into SC, respectively, which forms

https://doi.org/10.1021/jacs.5c22761
J. Am. Chem. Soc. 2026, 148, 6695−6703

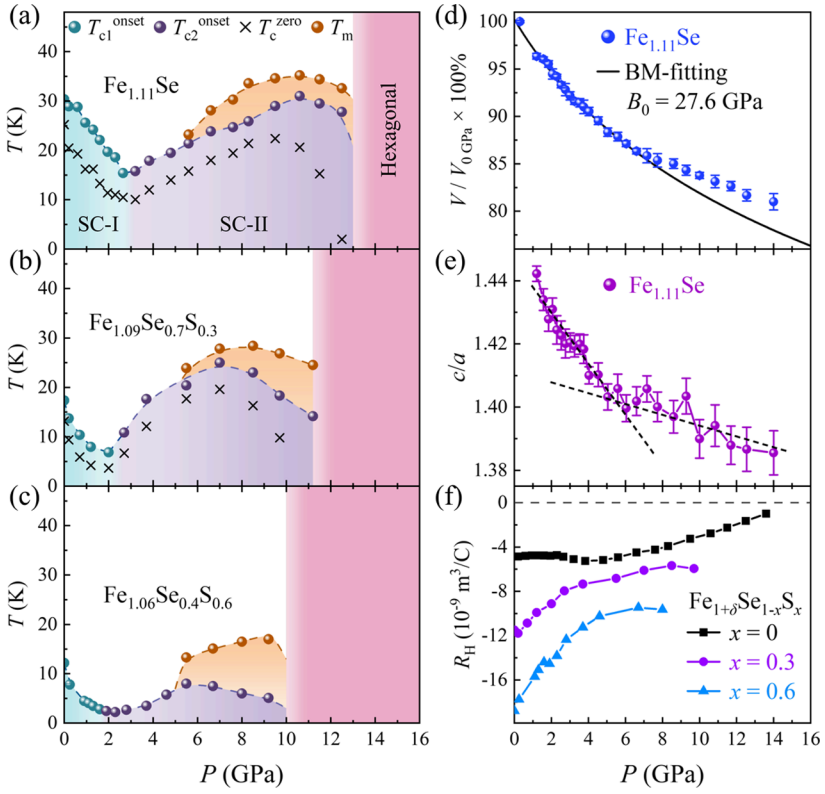

Figure 4. Phase diagram of pressurized $Fe_{1+\delta}Se_{1-x}S_x$ for (a) $x = 0$, (b) $x = 0.3$, and (c) $x = 0.6$. (d) Derived cell volume ratio V/V_{0GPa} and (e) lattice parameters ratio c/a for $Fe_{1.11}Se$. The gray line is a fitted curve by the Birch−Murnaghan (BM) equation of state. The black dashed lines guide the trend of c/a. (f) Pressure dependence of R_H at 50 K.

Table 1. Comparison of T_c and n_e at 50 K in Fe1.11Se, s-FeSe, and FeSe-Intercalates

	$Fe_{1.11}Se$	s-FeSe[1,8,47]	$K_xFe_2Se_2$[16,48,49]	$(Li_{0.8}Fe_{0.2})OHFeSe$[26,38]	$Li_x(NH_3)_yFe_2Se_2$[21,43]
T_c (K)	30.4	8.5	30.1	40	44.3
n_e ($\times 10^{21}$ cm^{-3})	1.28(1)	0.20(5)	0.7−1.2	1.60(1)	1.30(1)

a double-dome SC with a minimal T_c at $x \sim 0.2$. In the pressurized $K_xFe_2Se_2$, the T_c is first suppressed and then re-emerges at higher pressure. It is closely related to a so-called quantum critical point. In such two IBSCs, the crystal structures are flexible, and the geometry of the $FeAs_4/FeSe_4$ tetragonal is easy to modify upon chemical doping or pressure to some extent. Thus, the dominant contribution to the Fermi surface can shift between Fe $3d_{xy}$ and Fe $3d_{xz,yz}$, and thus, the induced Lifshitz transition may, in turn, determine the SC.

CONCLUSIONS

We have synthesized new $Fe_{1.11}Se$ single crystals that exhibit a T_c of 30.4 K utilizing a two-step hydrothermal ion-exchange and deintercalation process. Our comprehensive structural and spectroscopic analyses confirm the incorporation of 11% interstitial Fe2 ions. The pressure-induced evolution of SC in $Fe_{1.11}Se$ behaves like the FeSe-intercalates rather than binary s-FeSe. This work demonstrates the potential of a metastable strategy in searching high-T_c superconductors and inducing emergent physical properties in FeSe and other layered superconductors with weak interlayer force.

METHODS

Hydrothermal Synthesis of $Fe_{1.11}Se$ Single Crystals

$Fe_{1.11}Se$ single crystals were synthesized via a hydrothermal ion-exchange and deintercalation reaction process involving four sequential steps. First, high-purity tetragonal FeSe powder is obtained by melting Fe and Se pellets together in a quartz tube at 1100 °C and then annealing at 400 °C for 3−5 days. Then, high-quality single crystals of $K_{0.8}Fe_2Se_2$ were synthesized based on the methods described in ref 16. Subsequently, the as-grown $K_{0.8}Fe_2Se_2$ crystals, iron powders, and LiOH pellets were reacted in an aqueous medium within a sealed autoclave under high temperature and pressure, as described in ref 55. The golden-yellow $(Li_{1-y}Fe_y)OHFeSe$ ($y = 0.15$) single crystals were washed and collected. Finally, the $(Li_{1-y}Fe_y)$-OHFeSe crystals were placed in a Teflon-lined autoclave with 0.1 g of KOH, 0.3 g of Fe powder, 1 g of Sn powder, and 10 mL of deionized water. The mixture was heated at 120 °C for 3 days. The final $Fe_{1.11}Se$ crystals were collected from the aqueous solution, and the surface water was removed by vacuum evacuation. It yields large, air-stable, silver-white $Fe_{1.11}Se$ single crystals.

Structural and Chemical Characterization

Powder XRD measurements were performed on a Rigaku SmartLab diffractometer to evaluate the phase purity and orientation of single-crystal specimens. Chemical composition analysis was conducted using energy-dispersive X-ray spectroscopy (EDX) on pristine crystal surfaces and inductively coupled plasma-atomic emission spectroscopy (ICP-AES) on acid-dissolved samples. For structural determination, a single-crystal X-ray diffraction (XRD) measurement was

https://doi.org/10.1021/jacs.5c22761
J. Am. Chem. Soc. 2026, 148, 6695−6703

carried out at 299 K using a Bruker D8 diffractometer with Mo Kα radiation (λ = 0.71073 Å). Dynamic gas composition analysis of the $Fe_{1.11}Se$ single crystal during isothermal heating under high vacuum was performed via Quadrupole Mass Spectrometry (QMS). The local environment and valence state of iron atoms were investigated by ^{57}Fe Mössbauer spectroscopy at 23 K. *In situ* high-pressure synchrotron diffractions were carried out at the BL15U1 station of the Shanghai Synchrotron Radiation Facility (SSRF) by using a diamond anvil cell (DAC) with a facet diameter of 300 μm. The wavelength of the synchrotron beam is 0.6199 Å. Mineral oil served as the pressure-transmitting medium, and the pressure was calibrated by the standard ruby fluorescence method.

Magnetic and Electrical Transport Measurements

Magnetic properties were measured by using a superconducting quantum interference device (SQUID) magnetometer under an applied field of 10 Oe. Temperature-dependent electrical resistivity was measured using a standard four-probe configuration with applied currents below 2 mA. Hall coefficients (R_H) were determined from linear fits of the Hall resistivity (ρ_{xy}) versus magnetic field (H) in the range of −5 to +5 T at temperatures of 20, 40, 60, 80, 120, 160, 200, and 250 K. *In situ* high-pressure electrical transports were measured in a physical property measurement system (PPMS, Quantum Design, DynaCool). All measurements were carried out using a beryllium copper alloy DAC with a facet diameter of 500 μm, and the pressure was monitored with the ruby fluorescence method. We used KBr as both the pressure-transmitting and insulating medium.

DFT Calculation

First-principles calculations were carried out with the density functional theory (DFT) implemented in the Vienna ab initio simulation package (VASP).[56] The generalized gradient approximation (GGA) in the form of Perdew−Burke−Ernzerhof (PBE) was adopted for the exchange-correlation potentials.[57] We used the projector-augmented wave (PAW).[58,59] Because of random occupation of interstitial Fe2, we performed the calculations in a 2 × 2 × 1 supercell of FeSe ($P4/nmm$) and introduced 12.5% interstitial Fe to model Fe_9Se_8. The planewave energy cutoff was set to 900 eV, and the energy convergence criterion was set to 0.1 eV, using a Γ-centered 9 × 9 × 12 k-mesh for Brillouin-zone sampling.

■ ASSOCIATED CONTENT

Supporting Information

The Supporting Information is available free of charge at https://pubs.acs.org/doi/10.1021/jacs.5c22761.

Refinement results by SCXRD and PXRD (Tables S1 and S2); $\rho-T$ curves under fields, magnetic susceptibility, pressure-dependent $\rho-T$ curves for sulfur-doped samples, contour plots and fitting curves for synchrotron diffraction, details for Hall resistivity of all samples, band structure, and Fermi surface (PDF)

Accession Codes

Deposition Number 2524856 contains the supplementary crystallographic data for this paper. These data can be obtained free of charge via the joint Cambridge Crystallographic Data Centre (CCDC) and Fachinformationszentrum Karlsruhe Access Structures service.

■ AUTHOR INFORMATION

Corresponding Authors

Jian-gang Guo − *Beijing National Laboratory for Condensed Matter Physics, Institute of Physics, Chinese Academy of Sciences, Beijing 100190, China;* orcid.org/0000-0003-3880-3012; Email: jgguo@iphy.ac.cn

Shifeng Jin − *Beijing National Laboratory for Condensed Matter Physics, Institute of Physics, Chinese Academy of Sciences, Beijing 100190, China; School of Physical Sciences, University of Chinese Academy of Sciences, Beijing 100049, China; Hefei National Lab, Hefei 230088, China;* orcid.org/0000-0002-3522-1060; Email: shifengjin@iphy.ac.cn

Xiaolong Chen − *Beijing National Laboratory for Condensed Matter Physics, Institute of Physics, Chinese Academy of Sciences, Beijing 100190, China; School of Physical Sciences, University of Chinese Academy of Sciences, Beijing 100049, China;* Email: xlchen@iphy.ac.cn

Authors

Mingzhang Yang − *Beijing National Laboratory for Condensed Matter Physics, Institute of Physics, Chinese Academy of Sciences, Beijing 100190, China; College of Materials Science and Optoelectronic Technology, University of Chinese Academy of Sciences, Beijing 101408, China*

Yuxin Ma − *Beijing National Laboratory for Condensed Matter Physics, Institute of Physics, Chinese Academy of Sciences, Beijing 100190, China; School of Science, China University of Geosciences Beijing (CUGB), Beijing 100083, China*

Qi Li − *Beijing National Laboratory for Condensed Matter Physics, Institute of Physics, Chinese Academy of Sciences, Beijing 100190, China; College of Materials Science and Optoelectronic Technology, University of Chinese Academy of Sciences, Beijing 101408, China*

Ke Ma − *Beijing National Laboratory for Condensed Matter Physics, Institute of Physics, Chinese Academy of Sciences, Beijing 100190, China; School of Physical Sciences, University of Chinese Academy of Sciences, Beijing 100049, China*

Jiali Lu − *Beijing National Laboratory for Condensed Matter Physics, Institute of Physics, Chinese Academy of Sciences, Beijing 100190, China; College of Materials Science and Optoelectronic Technology, University of Chinese Academy of Sciences, Beijing 101408, China*

Zhaolong Liu − *Beijing National Laboratory for Condensed Matter Physics, Institute of Physics, Chinese Academy of Sciences, Beijing 100190, China; College of Materials Science and Optoelectronic Technology, University of Chinese Academy of Sciences, Beijing 101408, China*

Ruijin Sun − *School of Science, China University of Geosciences Beijing (CUGB), Beijing 100083, China;* orcid.org/0000-0001-5209-5257

Tianping Ying − *Beijing National Laboratory for Condensed Matter Physics, Institute of Physics, Chinese Academy of Sciences, Beijing 100190, China;* orcid.org/0000-0001-7665-1270

Mengdi Wang − *Key Laboratory of Quantum Materials under Extreme Conditions in Shandong Province, School of Physics and Physical Engineering, Qufu Normal University, Qufu 273165, China*

Xin Chen − *Key Laboratory of Quantum Materials under Extreme Conditions in Shandong Province, School of Physics and Physical Engineering, Qufu Normal University, Qufu 273165, China;* orcid.org/0000-0003-0652-0798

Changchun Zhao − *School of Science, China University of Geosciences Beijing (CUGB), Beijing 100083, China*

Complete contact information is available at: https://pubs.acs.org/10.1021/jacs.5c22761

https://doi.org/10.1021/jacs.5c22761
J. Am. Chem. Soc. 2026, 148, 6695−6703

Author Contributions

[▽]M.Y. and Y.M. contributed equally to this work. The manuscript was written through the contributions of all authors.

Notes

The authors declare no competing financial interest.

■ ACKNOWLEDGMENTS

We thank Jiazhen Zhang for the discussions. We thank Youting Song and Ziyan Lv for the SCXRD measurement. This work was financially supported by the National Key Research and Development Program of China (2023YFA1406301), Quantum Science and Technology National Science and Technology Major Project 2021ZD0302704, and the National Natural Science Foundation of China (52525205, 52272268, and 52250308). This work was supported by the Synergetic Extreme Condition User Facility (SECUF), including the High-pressure Synergetic Measurement Station and the Sample Preselection and Characterization Station. We thank the staff from Shanghai Synchrotron Radiation Facility (SSRF) at BL15U. It was also supported by the robotic AI-Scientist platform of the Chinese Academy of Sciences and the MatElab platform developed by the Condensed Matter Physics Data Center of the Chinese Academy of Sciences.

■ REFERENCES

(1) Hsu, F.-C.; Luo, J.-Y.; Yeh, K.-W.; Chen, T.-K.; Huang, T.-W.; Wu, P. M.; Lee, Y.-C.; Huang, Y.-L.; Chu, Y.-Y.; Yan, D.-C.; Wu, M.-K. Superconductivity in the PbO-Type Structure α-FeSe. *Proc. Natl. Acad. Sci. U.S.A.* **2008**, *105* (38), 14262−14264.

(2) Margadonna, S.; Takabayashi, Y.; T McDonald, M.; Kasperkiewicz, K.; Mizuguchi, Y.; Takano, Y.; Fitch, A. N.; Suard, E.; Prassides, K. Crystal Structure of the New $FeSe_{1-x}$ Superconductor. *Chem. Commun.* **2008**, *0* (43), 5607−5609.

(3) Liu, D.; Zhang, W.; Mou, D.; He, J.; Ou, Y.-B.; Wang, Q.-Y.; Li, Z.; Wang, L.; Zhao, L.; He, S.; Peng, Y.; Liu, X.; Chen, C.; Yu, L.; Liu, G.; Dong, X.; Zhang, J.; Chen, C.; Xu, Z.; Hu, J.; Chen, X.; Ma, X.; Xue, Q.; Zhou, X. J. Electronic Origin of High-Temperature Superconductivity in Single-Layer FeSe Superconductor. *Nat. Commun.* **2012**, *3* (1), No. 931.

(4) Ge, J.-F.; Liu, Z.-L.; Liu, C.; Gao, C.-L.; Qian, D.; Xue, Q.-K.; Liu, Y.; Jia, J.-F. Superconductivity above 100 K in Single-Layer FeSe Films on Doped $SrTiO_3$. *Nat. Mater.* **2015**, *14* (3), 285−289.

(5) Yin, J.-X.; Wu, Z.; Wang, J.-H.; Ye, Z.-Y.; Gong, J.; Hou, X.-Y.; Shan, L.; Li, A.; Liang, X.-J.; Wu, X.-X.; Li, J.; Ting, C.-S.; Wang, Z.-Q.; Hu, J.-P.; Hor, P.-H.; Ding, H.; Pan, S. H. Observation of a Robust Zero-Energy Bound State in Iron-Based Superconductor Fe(Te,Se). *Nat. Phys.* **2015**, *11* (7), 543−546.

(6) Wang, Z. F.; Zhang, H.; Liu, D.; Liu, C.; Tang, C.; Song, C.; Zhong, Y.; Peng, J.; Li, F.; Nie, C.; Wang, L.; Zhou, X. J.; Ma, X.; Xue, Q. K.; Liu, F. Topological Edge States in a High-Temperature Superconductor FeSe/$SrTiO_3$(001) Film. *Nat. Mater.* **2016**, *15* (9), 968−973.

(7) Zhang, P.; Yaji, K.; Hashimoto, T.; Ota, Y.; Kondo, T.; Okazaki, K.; Wang, Z.; Wen, J.; Gu, G. D.; Ding, H.; Shin, S. Observation of Topological Superconductivity on the Surface of an Iron-Based Superconductor. *Science* **2018**, *360* (6385), 182−186.

(8) McQueen, T. M.; Huang, Q.; Ksenofontov, V.; Felser, C.; Xu, Q.; Zandbergen, H.; Hor, Y. S.; Allred, J.; Williams, A. J.; Qu, D.; Checkelsky, J.; Ong, N. P.; Cava, R. J. Extreme Sensitivity of Superconductivity to Stoichiometry in $Fe_{1+\delta}Se$. *Phys. Rev. B* **2009**, *79* (1), No. 014522.

(9) Fang, M. H.; Pham, H. M.; Qian, B.; Liu, T. J.; Vehstedt, E. K.; Liu, Y.; Spinu, L.; Mao, Z. Q. Superconductivity Close to Magnetic Instability in $Fe(Se_{1-x}Te_x)_{0.82}$. *Phys. Rev. B* **2008**, *78* (22), No. 224503.

(10) Yeh, K.-W.; Huang, T.-W.; Huang, Y.; Chen, T.-K.; Hsu, F.-C.; M Wu, P.; Lee, Y.-C.; Chu, Y.-Y.; Chen, C.-L.; Luo, J.-Y.; Yan, D.-C.; Wu, M.-K. Tellurium Substitution Effect on Superconductivity of the α-Phase Iron Selenide. *EPL (Europhys. Lett.)* **2008**, *84* (3), No. 37002.

(11) Gresty, N. C.; Takabayashi, Y.; Ganin, A. Y.; McDonald, M. T.; Claridge, J. B.; Giap, D.; Mizuguchi, Y.; Takano, Y.; Kagayama, T.; Ohishi, Y.; Takata, M.; Rosseinsky, M. J.; Margadonna, S.; Prassides, K. Structural Phase Transitions and Superconductivity in $Fe_{1-\delta}Se_{0.57}Te_{0.43}$ at Ambient and Elevated Pressures. *J. Am. Chem. Soc.* **2009**, *131* (46), 16944−16952.

(12) Mizuguchi, Y.; Tomioka, F.; Tsuda, S.; Yamaguchi, T.; Takano, Y. Substitution Effects on FeSe Superconductor. *J. Phys. Soc. Jpn.* **2009**, *78* (7), No. 074712.

(13) Katayama, N.; Ji, S.; Louca, D.; Lee, S.; Fujita, M.; J Sato, T.; Wen, J.; Xu, Z.; Gu, G.; Xu, G.; Lin, Z.; Enoki, M.; Chang, S.; Yamada, K.; M Tranquada, J. Investigation of the Spin-Glass Regime between the Antiferromagnetic and Superconducting Phases in $Fe_{1+y}Se_xTe_{1-x}$. *J. Phys. Soc. Jpn.* **2010**, *79* (11), No. 113702.

(14) Hosoi, S.; Matsuura, K.; Ishida, K.; Wang, H.; Mizukami, Y.; Watashige, T.; Kasahara, S.; Matsuda, Y.; Shibauchi, T. Nematic Quantum Critical Point without Magnetism in $FeSe_{1-x}S_x$ Superconductors. *Proc. Natl. Acad. Sci. U.S.A.* **2016**, *113* (29), 8139−8143.

(15) Licciardello, S.; Buhot, J.; Lu, J.; Ayres, J.; Kasahara, S.; Matsuda, Y.; Shibauchi, T.; Hussey, N. E. Electrical Resistivity across a Nematic Quantum Critical Point. *Nature* **2019**, *567* (7747), 213−217.

(16) Guo, J.; Jin, S.; Wang, G.; Wang, S.; Zhu, K.; Zhou, T.; He, M.; Chen, X. Superconductivity in the Iron Selenide $K_xFe_2Se_2$ ($0 < x < 1.0$). *Phys. Rev. B***2010**, *82* (18), 180520. *Phys. Rev. B* **2010**, *82* (18), No. 180520.

(17) Fang, M.-H.; Wang, H.-D.; Dong, C.-H.; Li, Z.-J.; Feng, C.-M.; Chen, J.; Yuan, H. Q. Fe-Based Superconductivity with T_c=31 K Bordering an Antiferromagnetic Insulator in (Tl,K)Fe_xSe_2. *EPL (Europhys. Lett.)* **2011**, *94* (2), No. 27009.

(18) Wang, A. F.; Ying, J. J.; Yan, Y. J.; Liu, R. H.; Luo, X. G.; Li, Z. Y.; Wang, X. F.; Zhang, M.; Ye, G. J.; Cheng, P.; Xiang, Z. J.; Chen, X. H. Superconductivity at 32 K in Single-Crystalline $Rb_xFe_{2-y}Se_2$. *Phys. Rev. B* **2011**, *83* (6), No. 060512.

(19) Li, C.-H.; Shen, B.; Han, F.; Zhu, X.; Wen, H.-H. Transport Properties and Anisotropy of $Rb_{1-x}Fe_{2-y}Se_2$ Single Crystals. *Phys. Rev. B* **2011**, *83* (18), No. 184521.

(20) Ying, J. J.; Wang, X. F.; Luo, X. G.; Wang, A. F.; Zhang, M.; Yan, Y. J.; Xiang, Z. J.; Liu, R. H.; Cheng, P.; Ye, G. J.; Chen, X. H. Superconductivity and Magnetic Properties of Single Crystals of $K_{0.75}Fe_{1.66}Se_2$ and $Cs_{0.81}Fe_{1.61}Se_2$. *Phys. Rev. B* **2011**, *83* (21), No. 212502.

(21) Ying, T. P.; Chen, X. L.; Wang, G.; Jin, S. F.; Zhou, T. T.; Lai, X. F.; Zhang, H.; Wang, W. Y. Observation of Superconductivity at 30 ∼ 46 K in $A_xFe_2Se_2$(A = Li, Na, Ba, Sr, Ca, Yb and Eu). *Sci. Rep.* **2012**, *2* (1), No. 426.

(22) Ying, T.; Chen, X.; Wang, G.; Jin, S.; Lai, X.; Zhou, T.; Zhang, H.; Shen, S.; Wang, W. Superconducting Phases in Potassium-Intercalated Iron Selenides. *J. Am. Chem. Soc.* **2013**, *135* (8), 2951−2954.

(23) Guo, J.; Lei, H.; Hayashi, F.; Hosono, H. Superconductivity and Phase Instability of NH_3-Free Na-Intercalated $FeSe_{1-z}S_z$. *Nat. Commun.* **2014**, *5* (1), No. 4756.

(24) Hayashi, F.; Lei, H.; Guo, J.; Hosono, H. Modulation Effect of Interlayer Spacing on the Superconductivity of Electron-Doped FeSe-Based Intercalates. *Inorg. Chem.* **2015**, *54* (7), 3346−3351.

(25) Cassidy, S. J.; Woodruff, D. N.; Sedlmaier, S. J.; Blandy, J. N.; Reinhard, C.; Magdysyuk, O. V.; Goodwin, A. L.; Ramos, S.; Clarke, S. J. Stepwise Reactions in the Potassium and Ammonia-Intercalated Iron Selenide Superconductor Phase Diagram Followed by In Situ Powder Diffraction. *J. Am. Chem. Soc.* **2025**, *147* (22), 18563−18575.

https://doi.org/10.1021/jacs.5c22761
J. Am. Chem. Soc. 2026, 148, 6695−6703

(26) Lu, X. F.; Wang, N. Z.; Wu, H.; Wu, Y. P.; Zhao, D.; Zeng, X. Z.; Luo, X. G.; Wu, T.; Bao, W.; Zhang, G. H.; Huang, F. Q.; Huang, Q. Z.; Chen, X. H. Coexistence of Superconductivity and Antiferromagnetism in $(Li_{0.8}Fe_{0.2})$OHFeSe. *Nat. Mater.* **2015**, *14* (3), 325−329.
(27) Dong, X.; Zhou, H.; Yang, H.; Yuan, J.; Jin, K.; Zhou, F.; Yuan, D.; Wei, L.; Li, J.; Wang, X.; Zhang, G.; Zhao, Z. Phase Diagram of $(Li_{1-x}Fe_x)$OHFeSe: A Bridge between Iron Selenide and Arsenide Superconductors. *J. Am. Chem. Soc.* **2015**, *137* (1), 66−69.
(28) Wang, Q.-Y.; Li, Z.; Zhang, W.-H.; Zhang, Z.-C.; Zhang, J.-S.; Li, W.; Ding, H.; Ou, Y.-B.; Deng, P.; Chang, K.; Wen, J.; Song, C.-L.; He, K.; Jia, J.-F.; Ji, S.-H.; Wang, Y.-Y.; Wang, L.-L.; Chen, X.; Ma, X.-C.; Xue, Q.-K. Interface-Induced High-Temperature Superconductivity in Single Unit-Cell FeSe Films on $SrTiO_3$. *Chin. Phys. Lett.* **2012**, *29* (3), No. 037402.
(29) Lee, J. J.; Schmitt, F. T.; Moore, R. G.; Johnston, S.; Cui, Y.-T.; Li, W.; Yi, M.; Liu, Z. K.; Hashimoto, M.; Zhang, Y.; Lu, D. H.; Devereaux, T. P.; Lee, D.-H.; Shen, Z.-X. Interfacial Mode Coupling as the Origin of the Enhancement of T_c in FeSe Films on $SrTiO_3$. *Nature* **2014**, *515* (7526), 245−248.
(30) Mizuguchi, Y.; Tomioka, F.; Tsuda, S.; Yamaguchi, T.; Takano, Y. Superconductivity at 27K in Tetragonal FeSe under High Pressure. *Appl. Phys. Lett.* **2008**, *93* (15), No. 152505.
(31) Medvedev, S.; McQueen, T. M.; Troyan, I. A.; Palasyuk, T.; Eremets, M. I.; Cava, R. J.; Naghavi, S.; Casper, F.; Ksenofontov, V.; Wortmann, G.; Felser, C. Electronic and Magnetic Phase Diagram of β-$Fe_{1.01}Se$ with Superconductivity at 36.7 K under Pressure. *Nat. Mater.* **2009**, *8* (8), 630−633.
(32) Sun, J. P.; Matsuura, K.; Ye, G. Z.; Mizukami, Y.; Shimozawa, M.; Matsubayashi, K.; Yamashita, M.; Watashige, T.; Kasahara, S.; Matsuda, Y.; Yan, J.-Q.; Sales, B. C.; Uwatoko, Y.; Cheng, J.-G.; Shibauchi, T. Dome-Shaped Magnetic Order Competing with High-Temperature Superconductivity at High Pressures in FeSe. *Nat. Commun.* **2016**, *7* (1), No. 12146.
(33) Sun, J. P.; Ye, G. Z.; Shahi, P.; Yan, J.-Q.; Matsuura, K.; Kontani, H.; Zhang, G. M.; Zhou, Q.; Sales, B. C.; Shibauchi, T.; Uwatoko, Y.; Singh, D. J.; Cheng, J.-G. High-T_c Superconductivity in FeSe at High Pressure: Dominant Hole Carriers and Enhanced Spin Fluctuations. *Phys. Rev. Lett.* **2017**, *118* (14), No. 147004.
(34) Wang, P. S.; Sun, S. S.; Cui, Y.; Song, W. H.; Li, T. R.; Yu, R.; Lei, H.; Yu, W. Pressure Induced Stripe-Order Antiferromagnetism and First-Order Phase Transition in Fese. *Phys. Rev. Lett.* **2016**, *117* (23), No. 237001.
(35) Kothapalli, K.; Böhmer, A. E.; Jayasekara, W. T.; Ueland, B. G.; Das, P.; Sapkota, A.; Taufour, V.; Xiao, Y.; Alp, E.; Bud'ko, S. L.; Canfield, P. C.; Kreyssig, A.; Goldman, A. I. Strong Cooperative Coupling of Pressure-Induced Magnetic Order and Nematicity in FeSe. *Nat. Commun.* **2016**, *7* (1), No. 12728.
(36) Sun, L.; Chen, X.-J.; Guo, J.; Gao, P.; Huang, Q.-Z.; Wang, H.; Fang, M.; Chen, X.; Chen, G.; Wu, Q.; Zhang, C.; Gu, D.; Dong, X.; Wang, L.; Yang, K.; Li, A.; Dai, X.; Mao, H.; Zhao, Z. Re-Emerging Superconductivity at 48 K in Iron Chalcogenides. *Nature* **2012**, *483* (7387), 67−69.
(37) Guo, J.; Chen, X.-J.; Dai, J.; Zhang, C.; Guo, J.; Chen, X.; Wu, Q.; Gu, D.; Gao, P.; Yang, L.; Yang, K.; Dai, X.; Mao, H.; Sun, L.; Zhao, Z. Pressure-Driven Quantum Criticality in Iron-Selenide Superconductors. *Phys. Rev. Lett.* **2012**, *108* (19), No. 197001.
(38) Sun, J. P.; Shahi, P.; Zhou, H. X.; Huang, Y. L.; Chen, K. Y.; Wang, B. S.; Ni, S. L.; Li, N. N.; Zhang, K.; Yang, W. G.; Uwatoko, Y.; Xing, G.; Sun, J.; Singh, D. J.; Jin, K.; Zhou, F.; Zhang, G. M.; Dong, X. L.; Zhao, Z. X.; Cheng, J.-G. Reemergence of High-T_c Superconductivity in the $(Li_{1-x}Fe_x)OHFe_{1-y}Se$ under High Pressure. *Nat. Commun.* **2018**, *9* (1), No. 380.
(39) Shahi, P.; Sun, J. P.; Wang, S. H.; Jiao, Y. Y.; Chen, K. Y.; Sun, S. S.; Lei, H. C.; Uwatoko, Y.; Wang, B. S.; Cheng, J.-G. High-T_c Superconductivity up to 55 K under High Pressure in a Heavily Electron Doped $Li_{0.36}(NH_3)_yFe_2Se_2$ Single Crystal. *Phys. Rev. B* **2018**, *97* (2), No. 020508.
(40) Wang, X. C.; Liu, Q. Q.; Lv, Y. X.; Gao, W. B.; Yang, L. X.; Yu, R. C.; Li, F. Y.; Jin, C. Q. The Superconductivity at 18 K in LiFeAs System. *Solid State Commun.* **2008**, *148* (11), 538−540.
(41) Kiiamov, A. G.; Lysogorskiy, Y. V.; Vagizov, F. G.; Tagirov, L. R.; Tayurskii, D. A.; Croitori, D.; Tsurkan, V.; Loidl, A. Mössbauer Spectroscopy Evidence of Intrinsic Non-Stoichiometry in Iron Telluride Single Crystals. *Ann. Phys.* **2017**, *529* (4), No. 1600241.
(42) Kiiamov, A. G.; Tayurskii, D. A.; Vagizov, F. G.; Croitori, D.; Tsurkan, V.; von Nidda, H.-A. K.; Tagirov, L. R. DFT and Mössbauer Spectroscopy Study of a $FeTe_{0.5}Se_{0.5}$ Single Crystal. *JETP Lett.* **2019**, *109* (4), 266−269.
(43) Sun, S.; Wang, S.; Yu, R.; Lei, H. Extreme Anisotropy and Anomalous Transport Properties of Heavily Electron Doped $Li_x(NH_3)_yFe_2Se_2$ Single Crystals. *Phys. Rev. B* **2017**, *96* (6), No. 064512.
(44) Wang, Z.; Yuan, J.; Wosnitza, J.; Zhou, H.; Huang, Y.; Jin, K.; Zhou, F.; Dong, X.; Zhao, Z. The Upper Critical Field and Its Anisotropy in $(Li_{1-x}Fe_x)OHFe_{1-y}Se$. *J. Phys.: Condens. Matter* **2017**, *29* (2), No. 025701.
(45) Vedeneev, S. I.; Piot, B. A.; Maude, D. K.; Sadakov, A. V. Temperature Dependence of the Upper Critical Field of FeSe Single Crystals. *Phys. Rev. B* **2013**, *87* (13), No. 134512.
(46) Zhou, N.; Sun, Y.; Xi, C. Y.; Wang, Z. S.; Zhang, J. L.; Zhang, Y.; Zhang, Y. F.; Xu, C. Q.; Pan, Y. Q.; Feng, J. J.; Meng, Y.; Yi, X. L.; Pi, L.; Tamegai, T.; Xing, X.; Shi, Z. Disorder-Robust High-Field Superconducting Phase of FeSe Single Crystals. *Phys. Rev. B* **2021**, *104* (14), No. L140504.
(47) Ma, X.; Li, K.; Hou, S.; Mei, H.; Dong, Y.; Tan, M.; Xie, M.; Ren, W.; Jiang, X.; Li, Z.; Zhang, A.; Zhang, Q. Distinct Electronic Origins of Superconductivity and Nematicity in Fese. *Phys. Rev. Lett.* **2025**, *134* (25), No. 256002.
(48) Torchetti, D. A.; Fu, M.; Christensen, D. C.; Nelson, K. J.; Imai, T.; Lei, H. C.; Petrovic, C. ^{77}Se NMR Investigation of the $K_xFe_{2-y}Se_2$ Superconductor (T_c=33 K). *Phys. Rev. B* **2011**, *83* (10), No. 104508.
(49) Li, W.; Ding, H.; Deng, P.; Chang, K.; Song, C.; He, K.; Wang, L.; Ma, X.; Hu, J.-P.; Chen, X.; Xue, Q.-K. Phase Separation and Magnetic Order in K-Doped Iron Selenide Superconductor. *Nat. Phys.* **2012**, *8* (2), 126−130.
(50) Matsuura, K.; Mizukami, Y.; Arai, Y.; Sugimura, Y.; Maejima, N.; Machida, A.; Watanuki, T.; Fukuda, T.; Yajima, T.; Hiroi, Z.; Yip, K. Y.; Chan, Y. C.; Niu, Q.; Hosoi, S.; Ishida, K.; Mukasa, K.; Kasahara, S.; Cheng, J.-G.; Goh, S. K.; Matsuda, Y.; Uwatoko, Y.; Shibauchi, T. Maximizing T_c by Tuning Nematicity and Magnetism in $FeSe_{1-x}S_x$ Superconductors. *Nat. Commun.* **2017**, *8* (1), No. 1143.
(51) Mukasa, K.; Matsuura, K.; Qiu, M.; Saito, M.; Sugimura, Y.; Ishida, K.; Otani, M.; Onishi, Y.; Mizukami, Y.; Hashimoto, K.; Gouchi, J.; Kumai, R.; Uwatoko, Y.; Shibauchi, T. High-Pressure Phase Diagrams of $FeSe_{1-x}Te_x$: Correlation between Suppressed Nematicity and Enhanced Superconductivity. *Nat. Commun.* **2021**, *12* (1), No. 381.
(52) Izumi, M.; Zheng, L.; Sakai, Y.; Goto, H.; Sakata, M.; Nakamoto, Y.; Nguyen, H. L. T.; Kagayama, T.; Shimizu, K.; Araki, S.; Kobayashi, T. C.; Kambe, T.; Gu, D.; Guo, J.; Liu, J.; Li, Y.; Sun, L.; Prassides, K.; Kubozono, Y. Emergence of Double-Dome Superconductivity in Ammoniated Metal-Doped FeSe. *Sci. Rep.* **2015**, *5* (1), No. 9477.
(53) Iimura, S.; Matsuishi, S.; Sato, H.; Hanna, T.; Muraba, Y.; Kim, S. W.; Kim, J. E.; Takata, M.; Hosono, H. Two-Dome Structure in Electron-Doped Iron Arsenide Superconductors. *Nat. Commun.* **2012**, *3* (1), No. 943.
(54) Hiraishi, M.; Iimura, S.; Kojima, K. M.; Yamaura, J.; Hiraka, H.; Ikeda, K.; Miao, P.; Ishikawa, Y.; Torii, S.; Miyazaki, M.; Yamauchi, I.; Koda, A.; Ishii, K.; Yoshida, M.; Mizuki, J.; Kadono, R.; Kumai, R.; Kamiyama, T.; Otomo, T.; Murakami, Y.; Matsuishi, S.; Hosono, H. Bipartite Magnetic Parent Phases in the Iron Oxypnictide Superconductor. *Nat. Phys.* **2014**, *10* (4), 300−303.
(55) Sun, H.; Woodruff, D. N.; Cassidy, S. J.; Allcroft, G. M.; Sedlmaier, S. J.; Thompson, A. L.; Bingham, P. A.; Forder, S. D.;

https://doi.org/10.1021/jacs.5c22761
J. Am. Chem. Soc. 2026, 148, 6695−6703

Cartenet, S.; Mary, N.; Ramos, S.; Foronda, F. R.; Williams, B. H.; Li, X.; Blundell, S. J.; Clarke, S. J. Soft Chemical Control of Superconductivity in Lithium Iron Selenide Hydroxides $Li_{1-x}Fe_x(OH)Fe_{1-y}Se$. *Inorg. Chem.* **2015**, *54* (4), 1958−1964.
(56) Kresse, G.; Furthmüller, J. Efficient Iterative Schemes for Ab Initio Total-Energy Calculations Using a Plane-Wave Basis Set. *Phys. Rev. B* **1996**, *54* (16), No. 11169.
(57) Perdew, J. P.; Burke, K.; Ernzerhof, M. Generalized Gradient Approximation Made Simple. *Phys. Rev. Lett.* **1996**, *77* (18), No. 3865.
(58) Kresse, G.; Joubert, D. From Ultrasoft Pseudopotentials to the Projector Augmented-Wave Method. *Phys. Rev. B* **1999**, *59* (3), No. 1758.
(59) Kresse, G.; Furthmüller, J. Efficiency of Ab-Initio Total Energy Calculations for Metals and Semiconductors Using a Plane-Wave Basis Set. *Comput. Mater. Sci.* **1996**, *6* (1), 15−50.

https://doi.org/10.1021/jacs.5c22761
J. Am. Chem. Soc. 2026, 148, 6695−6703